Effect of grain size on strain rate sensitivity of cryomilled Al–Mg alloy

Byungmin Ahn[1], Rahul Mitra[2], Enrique J. Lavernia[3] and Steven R. Nutt[1]

(1) Department of Chemical Engineering and Materials Science, University of Southern California, Los Angeles, CA 90089-0241, USA
(2) Department of Metallurgical and Materials Engineering, Indian Institute of Technology, Kharagpur, India
(3) Department of Chemical Engineering and Materials Science, University of California, Davis, CA 95616-5294, USA

Abstract:

Al–Mg alloy powder was cryomilled to achieve a nanocrystalline (NC) structure having an average grain size of 50 nm with high thermal stability, and then consolidated by quasi-isostatic forging. The consolidation resulted in a bulk material with ultrafine grains of about 250 nm, and the material exhibited enhanced strength compared to conventionally processed Al–Mg alloy. The hardness of as-cryomilled powder, the forged ultrafine-grained (UFG) material, and the conventional coarse-grained (CG) alloy were measured by nanoindentation using various loading rates, and the results were compared with strain rate sensitivity (SRS) from uniaxial compression tests. Negative SRS was observed in the cryomilled NC powder and the forged UFG material, while the conventional alloy was relatively insensitive to strain rate. The dependence on loading rate was stronger in the NC powders than in the UFG material.

Key words: A-Short-Fibre Composites, C-Finite Element Analysis (FEA), C-Modelling, Mean-field homogenization

Membrane-type metamaterials: Transmission loss of multi-celled arrays
Naify, Christina J. and Chang, Chia-Ming and McKnight, Geoffrey and Scheulen, Florian and Nutt, Steven, Journal of Applied Physics, 109, 104902 (2011), DOI:http://dx.doi.org/10.1063/1.3583656

1. Introduction

Nanocrystalline (NC) and ultrafine-grained (UFG) materials produced by severe plastic deformation (SPD) methods have received great scientific interest because of their significantly enhanced strength and hardness compared to conventional coarse-grained (CG) materials [1, 2]. The enhanced properties of these materials are generally attributed to the reduced grain size, as expected from the Hall–Petch relationship, as well as high dislocation density. In conventional CG materials, the motion of lattice dislocations is the dominant mechanism of plastic deformation. However, materials with fine grains have higher concentrations of grain boundaries that inhibit dislocation motion, thereby increasing resistance to deformation.

Cryomilling involves ball-milling of metal powders in liquid nitrogen, and has been used to produce bulk NC materials with high thermal stability [3, 4]. During cryomilling, the powder particles are heavily deformed by the repeated impact of the balls, leading to an NC structure. The NC structure develops into an UFG structure when the powder is consolidated. The benefits of milling at cryogenic temperature include accelerated grain refinement, reduced oxygen contamination from the atmosphere, and reduced heat generation.

The effects of strain rate on deformation of bulk NC/UFG materials has been used to investigate mechanisms for improving the strength and ductility of the materials [5–11]. In general, NC metals show higher or lower strain rate sensitivity (SRS) compared to that of conventional CG materials, depending on the crystal structure [6, 9, 12, 13]. Usually an increase in the flow stress is observed at higher strain rates, indicative of positive SRS. According to previous studies, the effect of positive SRS becomes significant with decreasing grain size in face-centered cubic (FCC) metals [5–7], while body-centered cubic (BCC) metals exhibit decreased SRS with decreasing grain size [6, 9]. Recently,


negative SRS was reported in UFG Al–Mg alloys, along with serrated plastic flow [8], and this was attributed to dynamic strain aging. Similar negative SRS observed in BCC tantalum was attributed to twinning at higher strain rates [10].

Recent studies to estimate the SRS have involved either standard bulk specimen testing [6–8] or nanoindentation experiments [5, 10, 11, 14]. Nanoindentation measurements have been developed to measure mechanical properties locally in small regions, such as the cross-section of powder particles. In this study, the Al 5083 alloy specimens with nano-scale, ultrafine, and coarse grain sizes were subjected to nanoindentation at different loading rates and conventional compression testing to examine the effect of grain size on the SRS.

2. Experimental procedures

Gas-atomized Al–Mg alloy powder (Al 5083, Al–4.4Mg–0.7Mn–0.15Cr wt%, by Valimet, Inc.) was cryomilled in a 20-kg batch with liquid nitrogen for 8 h in a modified Szegvari attritor (DWA Aluminum Composites). Stainless steel balls were used with a ball-to-powder weight ratio of 32:1, and 40 g (0.2 wt%) of stearic acid was added into the milling chamber as a processing control agent. The process of cryomilling has been described in detail in an earlier report [15]. The cryomilled powder was hot vacuum degassed at 10−5 Torr and 450°C (ramp rate of 1°C/min and dwell time of 45 h). For consolidation, the degassed powder was heated to 450°C and subsequently forged (Advanced Materials & Manufacturing Technologies, LLC). The maximum pressure applied to the die was 343 MPa. The forged disk was machined to remove the canning material, then quasi-isostatically forged once again. Final dimensions of the disk were 128 mm (diameter) × 16 mm

(thickness). A standard Al 5083-H131 'armor grade' plate was used for comparison. The plate was made by casting, followed by hot rolling, and then cold working to the H131 condition.

The concentration of metallic alloying elements was measured using DC plasma emission spectroscopy (by Luvak, Inc.) according to ASTM E1097-03. Non-metallic elements were measured by inert gas fusion methods (RH404 (H), and TCH600 (O and N) analyzers) and by combustion combined with IR detection (CS600 (C) analyzer, LECO, Inc). Samples of the materials, both as-cryomilled powder and forged Al 5083 plate, were prepared for transmission electron microscopy (TEM, Philips EM-420) examination. Cryomilled powders were prepared by mixing with an epoxy (G-1, Gatan Inc) and curing at ambient temperature, then ground, polished, dimpled, and ion milled to perforation for electron transparency. TEM samples from the forged plate were prepared by electrolytic jet polishing using an ethanol solution containing 8% perchloric acid + 10% 2-butoxyethanol at a temperature of −5°C. Grain size of as-cryomilled powder and forged plate was measured directly from the TEM micrographs using 350 individual grains. For the cryomilled powder, the grain size measurements were performed on 6–7 powder particles. The mean grain size of the standard Al 5083 plate was obtained from the electron backscattered detector (EBSD, Oxford Nordlys F400) attached to a field emission scanning electron microscope (FE-SEM, Zeiss 1550VP). The EBSD specimen of the standard CG plate was prepared using a broad ion beam cross-section polisher (JEOL CP SM-09010) utilizing a low-voltage Ar ion beam (5 kV).

The hardness measurements were performed using a nanoindenter (TriboIndenter, Hysitron) with a 100-nm Berkovich tip. Tests were carried out on resin-mounted Al–Mg alloy samples of the cryomilled NC powder, the forged UFG plate, and the conventional CG plate. The loading rates were varied between 50 and 50,000 μN/s without holding segment, and the maximum load used for

each test was 5,000 μN. About 25–50 indents were performed at each indentation loading rate for each specimen. During the tests, the standard nanoindentation drift correction software was applied. The room temperature uniaxial compression tests were conducted for the UFG and CG materials using an electromechanical testing system (Instron 5567) with cubic samples of 5 mm on each side.

3. Results

The typical grain structures of the as-cryomilled NC powder, the forged UFG plate, and the rolled CG plate appear in Fig. 1a, b, and c, respectively. For the NC and UFG materials, the selected area diffraction (SAD) patterns are displayed in the corresponding TEM bright field micrographs, as shown in Fig. 1a and b, respectively. The as-cryomilled powder consisted of mostly equiaxed NC grains with an average grain size of 50 nm. The uniform rings in the SAD pattern shown in Fig. 1a are indicative of randomly oriented fine grains. In contrast, discontinuous rings consisting of individual spots were observed in the SAD patterns from the forged UFG material, as shown in Fig. 1b. The spots in the SAD pattern arose from individual CGs. The average grain size of the UFG material was 252 nm. The greater average grain size in the forged UFG plate (252 nm) compared to that in the cryomilled NC powder (50 nm) is attributed to grain coarsening during high-temperature degassing and consolidation. The histograms of the grain size distribution and aspect ratios of the as-cryomilled NC powder were reported in a previous study [16]. Figure 1c shows an EBSD grain map superimposed on an SEM micrograph of the CG plate of conventional Al 5083. The average grain size of the CG material as obtained from EBSD was 140 μm. The grain size statistics of all three materials is summarized in Table 1.

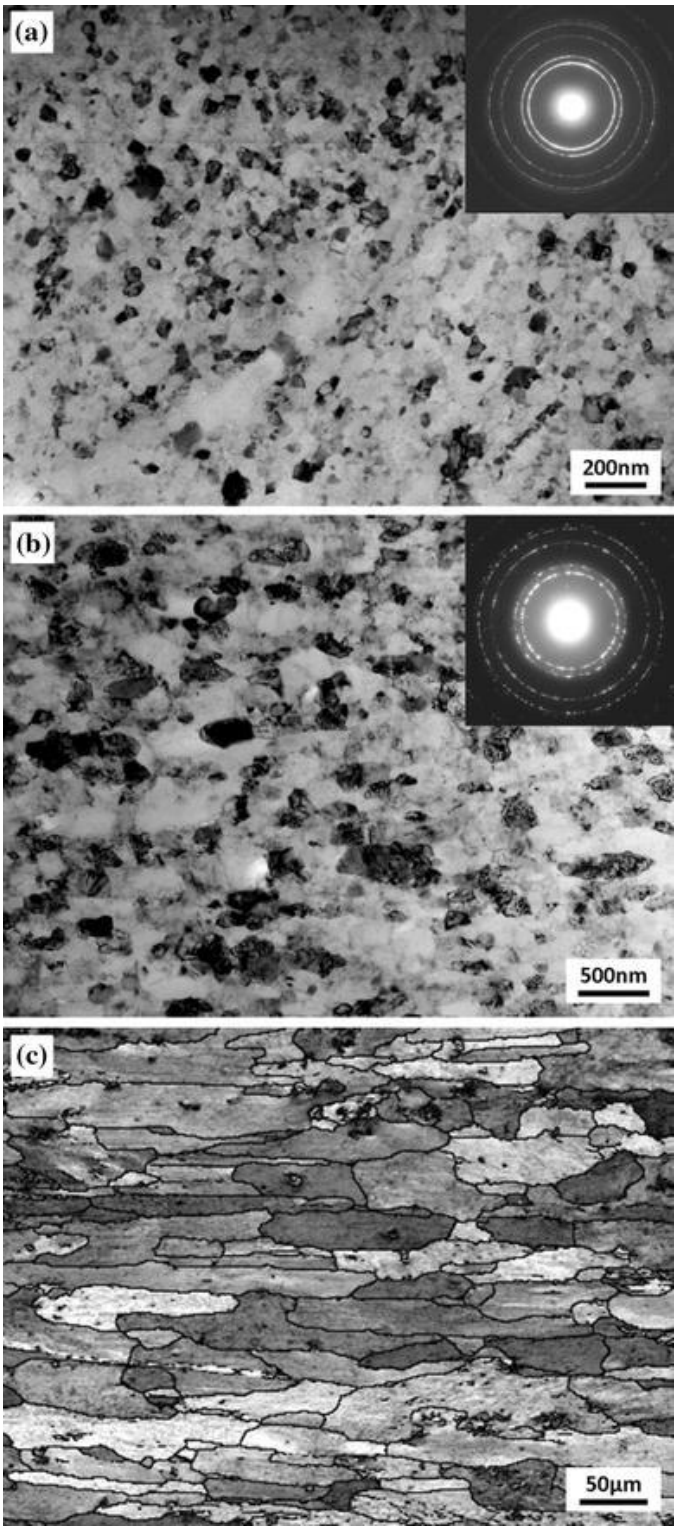

Fig. 1 *Microstructure of* ***a*** *as-cryomilled NC powder (TEM BF, SAD),* ***b*** *forged UFG plate (TEM BF, SAD), and* ***c*** *conventional CG plate (SEM, EBSD grain map)*

Effect of grain size on strain rate sensitivity of cryomilled Al-Mg alloy" B. Ahn, R Mitra, EJ Lavernia, SR Nutt, J Mater Sci 45 (2010) 4790-4795. DOI<http://dx.doi.org/10.1007/s10853-010-4664-4>

Table 1 Mean grain size of as-cryomilled NC powder, forged UFG plate, and CG plate

Materials	Average grain size	Measurement method
As-cryomilled NC powder	50 ± 33 nm	Individual grains from TEM
Forged UFG plate[a]	252 ± 130 nm	Individual grains from TEM
Conventional CG plate[b]	140 μm	EBSD

[a]Viewed normal to the forging direction; [b] viewed normal to the rolling direction

The composition of the forged UFG plate is shown in Table 2, along with the nominal composition of standard Al 5083 alloy. The concentration of metallic alloying elements of the UFG plate was within the specification range for Al 5083. However, the concentrations of the non-metallic elements, N, H, O, and C, were much greater in the forged UFG plate produced from cryomilled powder than those in conventionally processed Al 5083 alloy, as shown in Table 2. Excess nitrogen was incorporated during cryomilling in liquid nitrogen, while excess hydrogen was introduced via the processing control agent, stearic acid ($C_{18}H_{36}O_2$), and by reaction of the powder with moisture in the surrounding atmosphere. Excess oxygen arose mainly from oxidation of the powder, and the carbon resulted also from breakdown of the stearic acid. TEM studies and chemical analyses have shown evidence for the presence of nitrides, carbides, or oxides [*17*], although a significant portion of the N, H, O, and C are expected to be present as interstitial atoms or as non-grain boundary solute in the Al 5083 alloy. Thermodynamics calculations indicate that high-angle grain boundaries are potential sites for solute segregation in general [*18–20*].

Table 2 Composition of the forged Al 5083 alloy, compared with the specification for the standard Al 5083 [15]

Materials	Al (wt %)	Mg (wt %)	Mn (wt %)	Fe (wt %)	Cr (wt %)	N (wt%)	H (ppm)	O (wt %)	C (wt %)
Forged UFG plate	92.5	4.46	0.65	0.29	0.07	0.56	27	0.48	0.15
Specification for Al 5083	92.4–95.6	4.0–4.9	0.4–1.0	0.4 max	0.05–0.25	<0.0005[a]	1.3[a]	0.003[a]	0.001[a]

[a]*Non-metallic elements measured from a standard Al 5083 plate*

Figure 2 shows load versus displacement (*P–h*) curves of all three materials obtained from different indentation loading rates. The average value of the final indentation depth varies with materials, ~200 nm (NC powder), ~260 nm (UFG plate), and ~320 nm (CG plate), elucidating the effects of grain size on indentation behavior. Both the loading and unloading segments of the curves were shifted in the NC powder and in the UFG plate depending on the loading rates, as shown in Fig. 2a and b, while relatively minor variation was observed in the CG plate in Fig. 2c. Such variations in the loading and unloading curves are due to different displacements of the indenter at different loading rates for the same maximum load (≈5,000 μN). The variation is more significant in the NC powder than in the UFG plate, indicating that finer grain sizes (<100 nm) give rise to greater SRS.

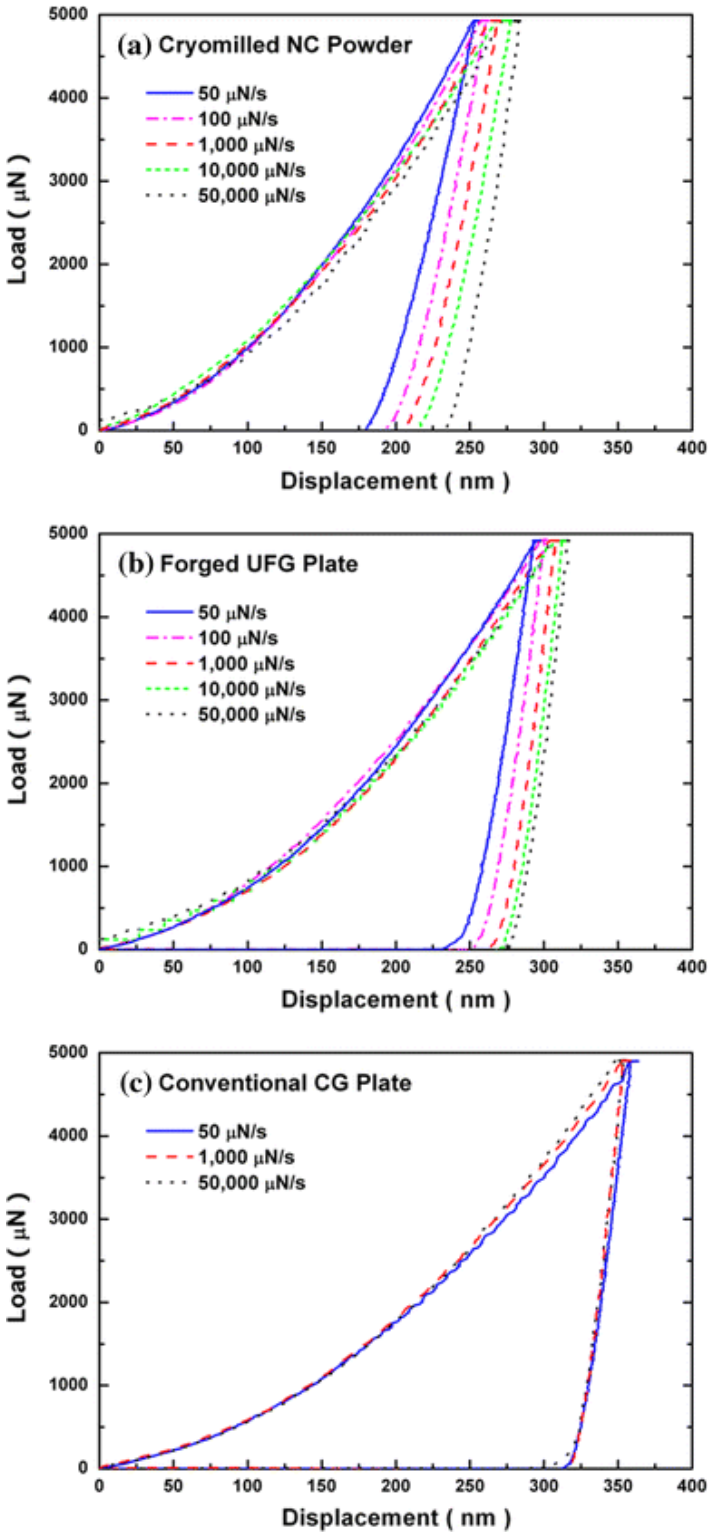

Fig. 2 Load versus displacement curves performed at different loading rates for a as-cryomilled NC powder, b forged UFG plate, and cconventional CG plate

Effect of grain size on strain rate sensitivity of cryomilled Al-Mg alloy" B. Ahn, R Mitra, EJ Lavernia, SR Nutt, J Mater Sci 45 (2010) 4790-4795. DOI<http://dx.doi.org/10.1007/s10853-010-4664-4>

Hardness variations as a function of loading rate (50–50,000 μN/s) are plotted for all three materials in Fig. 3. The standard deviations are indicated as error bars for each loading rate and material. The following observations can be made after careful examination of the plots: (i) the hardness decreases with increasing loading rate for the NC powder and the UFG material, while it remains virtually constant for the CG material; (ii) the decrease in hardness with increasing loading rate is much more pronounced for the NC powder than for the UFG material; (iii) the hardness drop with increasing loading rate for the NC powder and the UFG material is largest at the lower loading rates; (iv) the standard deviations of the hardness values are greater for the cryomilled NC powder and the forged UFG material than for the conventional CG material; and (v) the average hardness of the NC powder is 2–2.5 times greater than the CG alloy, depending on the loading rate. The higher hardness values in materials with finer grain sizes follow expectations based on the Hall–Petch relationship. The greater standard deviations for hardness values obtained from the cryomilled NC powder and the forged UFG sample are attributed to microstructural inhomogeneity, particularly due to the breadth of the grain size distributions. The decrease in the hardness with loading rate indicates negative SRS in this alloy, particularly when the average grain size is less than 100 nm, while negligible strain rate dependence is observed in the conventional CG alloy.

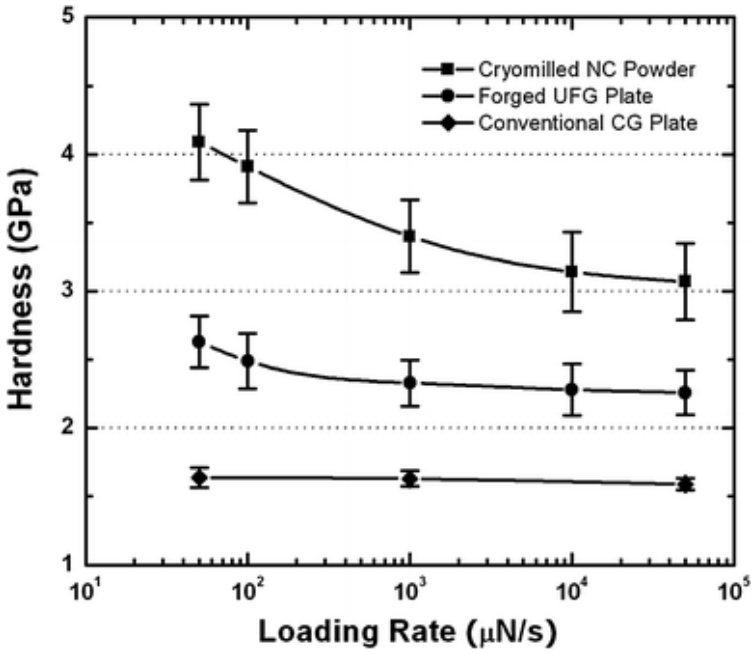

Fig. 3 Hardness variations of the as-cryomilled NC powder, forged UFG, and conventional CG plate measured by nanoindentation

Figure 4 shows plots of compressive yield strength against strain rate for the forged UFG and conventional CG plates. Comparison of the plots shows: (i) the yield strength of the forged UFG material is roughly 2× greater; and (ii) the SRS exponent (m) of the UFG material is slightly negative ($m = -0.0108$), while that of the CG material is smaller and positive ($m = 0.0025$). The higher yield strength and negative SRS of the UFG alloy are consistent with results from the nanoindentation hardness measurements depicted in Figs. 2 and 3. Typical true stress–true strain curves for the forged UFG and CG materials recorded for tests carried out at strain rates of 10^{-1}, 10^{-3}, and 10^{-5} s^{-1} are shown in Fig. 5. The stress–strain curves indicate that the strain hardening rates are independent of strain rate.

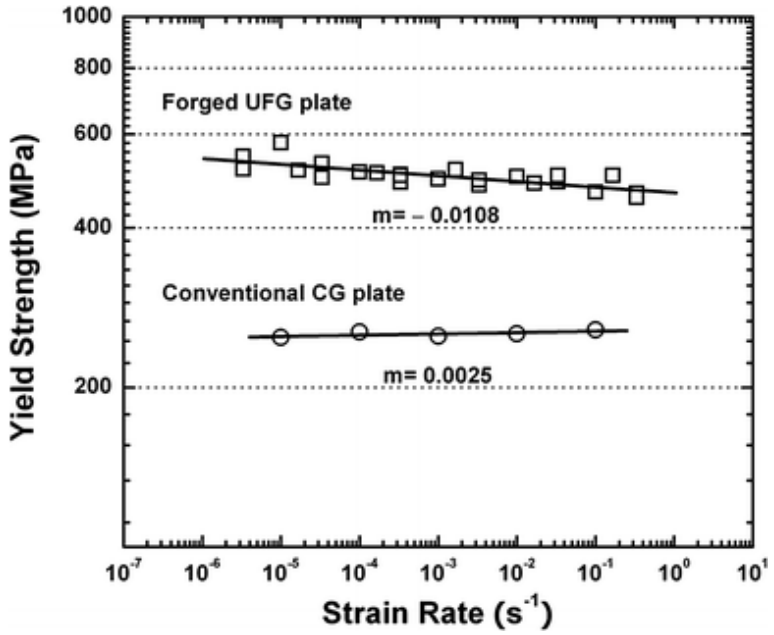

Fig. 4 Strain rate sensitivity of the UFG plate and conventional CG plate

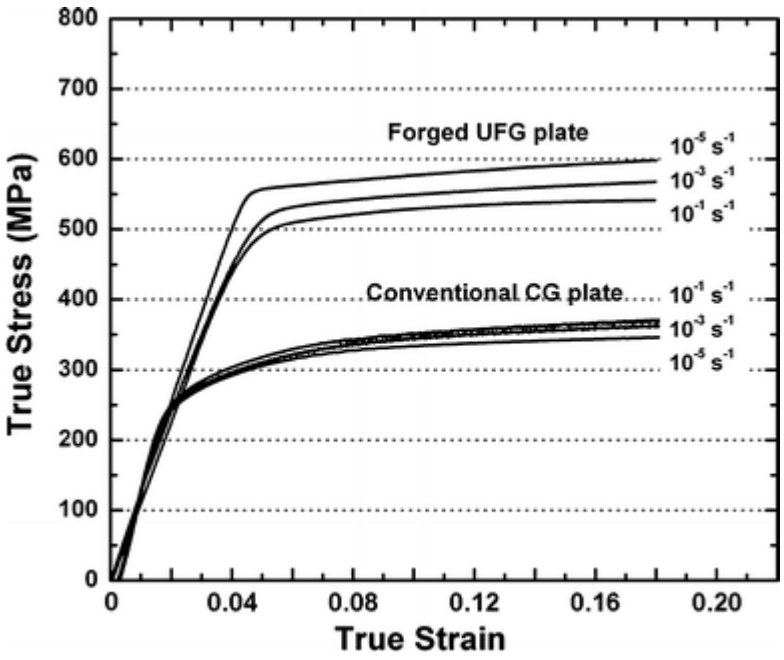

Fig. 5 Compressive behavior of the UFG plate and conventional CG plate at different strain rates

Effect of grain size on strain rate sensitivity of cryomilled Al-Mg alloy" B. Ahn, R Mitra, EJ Lavernia, SR Nutt, J Mater Sci 45 (2010) 4790-4795. DOI<http://dx.doi.org/10.1007/s10853-010-4664-4>

4. Discussion

The negative SRS observed during nanoindentation experiments and compression tests for the NC and UFG materials differs from the behavior reported for the FCC metals and alloys [*6*]. Negative SRS is usually observed in materials exhibiting dynamic strain aging [*8*, *21*], a phenomenon typically caused by the attractive interaction of dislocations and interstitial solute atoms, including nitrogen, carbon, hydrogen, and oxygen. Pinning of dislocations by interstitial solute atoms causes jerky glide of dislocations. However, at high loading rates or strain rates, there is a rapid increase in the density of mobile dislocations, particularly dislocations that were previously locked in and were not free to move otherwise. The larger plastic deformation accompanying the generation of increased density of mobile dislocations is manifest during nanoindentation as larger indentation sizes and lower hardness values, and in lower yield strength values in compression tests.

Both the density of dislocations and their mobility decrease as the grain size decreases, and this is particularly pronounced when the average grain size is less than 100 nm. Hence, the effect of higher loading rates on triggering of dislocation motion is more pronounced when the grain size is in the NC range. In NC and UFG materials, the grain boundaries act both as principal sources and sinks for dislocations [*22*, *23*]. As the grain boundaries are enriched with solute atoms, the solute–dislocation interaction is expected to increase with decreasing grain size. The fact that negative SRS is more pronounced in indentation tests with lower loading rates is intriguing, and suggests that thermally activated grain boundary diffusion is involved in the deformation at lower strain rates, in addition to dislocation glide. The higher hardness and/or strength values observed at lower strain rates implies that the solute atoms are able to diffuse short distances to dislocation cores and form Cottrel-type atmospheres, restricting their motion. Hence, the drag of solute atoms on mobile

dislocations is significant at lower strain rates. The activation volume v^* has been calculated using the relationship [*9*, *11*]:

$$v* = \frac{33\sqrt{kT}}{Hm} \quad (1)$$

where, k is the Boltzmann constant (JK^{-1}), T is the temperature (K), H is the hardness (Nm^{-2}), and m is the SRS exponent. Using the average hardness values obtained at the highest loading rate and the absolute values of m, the activation volumes of the UFG and CG materials are determined to be 32 b^3 and 220 b^3, respectively. If the SRS of the NC material is assumed to be similar to that of UFG, the activation volume is about 20 b^3. As the experimental observations suggest that the absolute value of the SRS of the NC material is greater than that of UFG material, the actual activation volume is expected to be less than 20 b^3. Activation volumes in the range (<100 b^3) in case of the NC and UFG materials suggest that deformation is controlled by dislocation glide affected by the Peierls type barrier caused by the presence of atmosphere of solute atoms at the dislocation core [*24*, *25*]. On the other hand, the much greater activation volume (>100 b^3) of the CG material indicates the involvement of dislocation intersections in deformation, as expected [*24*].

5. Conclusions

The effect of grain size on the SRS of the Al–Mg alloy (Al 5083) was examined using nano-indentation at different loading rates (50–50,000 μN/s), and by uniaxial compression tests with strain rates between 10^{-6} and 1 s^{-1}. The negative SRS was more pronounced in the NC powder than in the UFG material, while it was slightly positive in the conventional CG alloy. The negative SRS in the NC and UFG materials was attributed to pinning of dislocations by interstitial solute atoms as well as the small grain size, both of which restrict dislocation motion. Indentation at higher loading rates

is expected to trigger dislocation motion by unlocking from solute atoms, increasing the density of mobile dislocations and causing greater plastic deformation for a given load. The negative SRS was more pronounced at lower loading rates during nanoindentation, suggesting that thermally activated grain boundary diffusion of solute atoms has an important role in pinning dislocations. The activation volumes of the NC and UFG materials suggest that overcoming the Peierls type barrier caused due to pinning by solute atoms is rate-controlling, while that of the CG material indicates that dislocation intersections are involved.

Acknowledgements: Research was sponsored by U.S. Army Research Laboratory (ARL) and was accomplished under Cooperative Agreement W911NF-08-2-0028. The views and conclusions made in this document are those of the authors and should not be interpreted as representing the official policies, either expressed or implied, of ARL or the U.S. Government. The U.S. Government is authorized to reproduce and distribute reprints for Government purposes notwithstanding any copyright notation hereon. The authors are grateful to JEOL USA, Inc. for providing access to the SM-09010 cross-section polisher, to Scott Sitzman (Oxford Instruments America, Inc.) for his effort on EBSD analysis, to Prof. Andrea Hodge (University of Southern California) for her permission to use the nanoindenter, and to Prof. Kwang Ho Kim (National Core Research Center for Hybrid Materials Solution, Busan, Korea) for valuable technical discussions. The authors also gratefully acknowledge A. Piers Newbery previously of University of California, Davis, for his assistance.

References:

1. Gleiter H (1989) Prog Mater Sci 33:223
2. Kumar KS, Van Swygenhoven H, Suresh S (2003) Acta Mater 51:5743
3. Zhou F, Lee J, Dallek S, Lavernia EJ (2001) J Mater Res 16:3451
4. Witkin DB, Lavernia EJ (2006) Prog Mater Sci 51:1
5. Schwaiger R, Moser B, Dao M, Chollacoop N, Suresh S (2003) Acta Mater 51:5159
6. Wei Q, Cheng S, Ramesh KT, Ma E (2004) Mater Sci Eng A 381:71
7. Han BQ, Huang JY, Zhu YT, Lavernia EJ (2006) Scripta Mater 54:1175

8. Han BQ, Huang J, Zhu YT, Lavernia EJ (2006) Adv Eng Mater 8:945
9. Wei Q (2007) J Mater Sci 42:1709. doi:10.1007/s10853-006-0700-9
10. Wang YM, Hodge AM, Bythrow PM, Barbee TW Jr, Hamza AV (2006) Appl Phys Lett 89:081903
11. Cavaliere P (2008) Physica B 403:569
12. Masumura RA, Hazzledine PM, Pande CS (1998) Acta Mater 46:4527
13. Hayes RW, Witkin D, Zhou F, Lavernia EJ (2004) Acta Mater 52:4259
14. Qian T, Marx M, Schűler K, Hockauf M, Vehoff H (2010) Acta Mater 58:2112
15. Newbery AP, Ahn B, Hayes RW, Pao PS, Nutt SR, Lavernia EJ (2008) Metall Mater Trans A 39A:2193
16. Ahn B, Newbery AP, Lavernia EJ, Nutt SR (2007) Mater Sci Eng A 463:61
17. Li Y, Liu W, Ortalan V, Li WF, Zhang Z, Vogt R, Browning ND, Lavernia EJ, Schoenung JM (2010) Acta Mater 58:1732
18. Dregia SA, Wynblatt P (1991) Acta Metall Mater 39(5):771
19. Hondros ED, Seah MP (1977) Inter Mater Rev 22:262
20. McLean D (1957) Grain boundaries in metals. Clarendon Press, Oxford, p 116
21. Fan GJ, Wang GY, Choo H, Liaw PK, Park YS, Han BQ, Lavernia EJ (2005) Scripta Mater 52:929
22. Li JCM (1963) Trans Met Soc AIME 227:239
23. Yamakov V, Wolf D, Philpot SR, Mukherjee AK, Gleiter H (2002) Nat Mater 1:1
24. Conrad H (1964) J Metals 16(7):582
25. Lothe J (1962) Acta Metall 10:663